Biomaterials xxx (2010) 1–8

Contents lists available at ScienceDirect

Biomaterials

journal homepage: www.elsevier.com/locate/biomaterials

In vitro hemocompatibility of thin film nitinol in stenotic flow conditions

C.P. Kealey [a,*], S.A. Whelan [a], Y.J. Chun [b], C.H. Soojung [b], A.W. Tulloch [a], K.P. Mohanchandra [b], D. Di Carlo [c], D.S. Levi [d], G.P. Carman [b], D.A. Rigberg [a]

[a] David Geffen School of Medicine, Department of Surgery, Division of Vascular Surgery, University of California, Los Angeles, CA, USA
[b] Henry Samueli School of Engineering, Department of Mechanical and Aerospace Engineering, University of California, Los Angeles, CA, USA
[c] Henry Samueli School of Engineering, Department of Biomedical Engineering, University of California, Los Angeles, CA, USA
[d] David Geffen School of Medicine, Department of Pediatrics, Division of Interventional Cardiology, University of California, Los Angeles, CA, USA

ARTICLE INFO

Article history:
Received 2 June 2010
Accepted 7 August 2010
Available online xxx

Keywords:
Nitinol
Thin
Film
Hemocompatibility
Endovascular
Stent

ABSTRACT

Because of its low profile and biologically inert behavior, thin film nitinol (TFN) is ideally suited for use in construction of endovascular devices. We have developed a surface treatment for TFN designed to minimize platelet adhesion by creating a superhydrophilic surface. The hemocompatibility of expanded polytetrafluorethylene (ePTFE), untreated thin film nitinol (UTFN), and a surface treated superhydrophilic thin film nitinol (STFN) was compared using an *in vitro* circulation model with whole blood under flow conditions simulating a moderate arterial stenosis. Scanning electron microscopy analysis showed increased thrombus on ePTFE as compared to UTFN or STFN. Total blood product deposition was 6.3 ± 0.8 mg/cm^2 for ePTFE, 4.5 ± 2.3 mg/cm^2 for UTFN, and 2.9 ± 0.4 mg/cm^2 for STFN ($n = 12$, $p < 0.01$). ELISA assay for fibrin showed 326 ± 42 μg/cm^2 for ePTFE, 45.6 ± 7.4 μg/cm^2 for UTFN, and 194 ± 25 μg/cm^2 for STFN ($n = 12$, $p < 0.01$). Platelet deposition measured by fluorescent intensity was 79,000 20,000 AU/mm^2 for ePTFE, 810 ± 190 AU/mm^2 for UTFN, and 1600 ± 25 AU/mm^2 for STFN ($n = 10$, $p < 0.01$). Mass spectrometry demonstrated a larger number of proteins on ePTFE as compared to either thin film. UTFN and STFN appear to attract significantly less thrombus than ePTFE. Given TFN's low profile and our previously demonstrated ability to place TFN covered stents *in vivo*, it is an excellent candidate for use in next-generation endovascular stents grafts.

1. Introduction

Expanded polytetrafluorethylene (ePTFE) has been used for decades as an artificial conduit for vascular bypass grafts. More recently, it has become the most commonly used material for covering stents [1]. These covered stent grafts have been extremely successful at treating aneurysms of the thoracic and abdominal aorta and have dramatically decreased the need for large open surgical procedures [2–4]. As small diameter ePTFE covered stents have become available, their use has expanded to include treatment of atherosclerotic disease in the arteries of the pelvis and lower extremities. While ePTFE covered stents have shown some success in these smaller vessels, there are still significant technical challenges and limitations to their use. For example, restenosis rates for ePTFE are approximately 30% after 12 months, and this rate is known to increase as the length of the lesion being treated increases or as the diameter of the vessel decreases [5–10]. Other disadvantages include a relatively rough surface, bulky delivery catheters double the size of those required for a comparable bare metal stents, and slow or non-existent endothelialization [11–15]. Therefore, there is an acute need to develop new biomaterials that are less thrombogenic, less bulky, and more easily endothelialized than the ePTFE currently used to cover stents.

Thin film nitinol (TFN defined as thickness less than 10 microns) is a nickel titanium alloy with a number of qualities that suggest it may be advantageous for use in blood contacting devices. Bulk nitinol (dimensions greater than 30 microns) has a long history of implantation in human beings and is currently the most common material used to manufacture stents due to its superelastic and temperature dependant shape memory properties. TFN retains the superelastic and shape memory properties indicative of bulk nitinol and also has a large tensile strength (500 MPa). TFN is manufactured in sheets between 1 and 10 μm thick with an average surface roughness of 5 nm as compared to surface roughness of most electropolished stents of 500 nm [16–18]. Its extremely low profile adds almost no bulk to the catheters used for endovascular delivery, and its smooth surface portends a favorable hemocompatibility profile as surface roughness is known to correlate with thrombogenicity

* Corresponding author. Tel.: +1 310 206 5109; fax: +1 310 206 0138.
E-mail address: ckealey@mednet.ucla.edu (C.P. Kealey).

0142-9612/$ – see front matter © 2010 Elsevier Ltd. All rights reserved.
doi:10.1016/j.biomaterials.2010.08.014

[11,12]. TFN may also be produced in a variety of shapes and sizes, and is not susceptible to the calcification commonly observed with ePTFE implants.

Previously, our group reported surface modifications to TFN that yielded a material with a contact wetting angle of 0° [18]. The "superhydrophilic" TFN (STFN) was designed to improve hemocompatibility as native endothelium is known to be both negatively charged and hydrophilic. Indeed, a recently published study of STFN showed dramatically decreased platelet adhesion and aggregation as compared to either ePTFE or untreated TFN (UTFN) [19]. The purpose of this study was to construct a more realistic model of the *in vivo* thrombotic response to TFN. We, therefore, developed an *in vitro* circulation model capable of circulating fresh whole blood under wall shear conditions simulating a moderate arterial stenosis. Using this model, we developed a series of assays to qualitatively and quantitatively examine experimentally formed thrombi. These techniques were then applied to prototype TFN covered stents with ePTFE covered stents serving as control.

2. Materials and methods

2.1. Thin film nitinol creation

The fabrication process for TFN used in this study has been described in detail previously [20]. Briefly, the 6 μm thick films were deposited on a 4 inch silicon wafer buffered with a 500 nm silicon oxide layer. Following deposition and removal of the film from the silicon oxide layer, the film was crystallized for 120 min at 500 °C in a vacuum of less than 1×10^{-7} torr. The TFN material used for this study had an austenite finish temperature of approximately 34 °C. In all tests conducted in this study, the TFN was in its austenite phase. All films underwent a final cleaning treatment consisting of sequential rinsing in acetone, methanol, and ethanol for 5 min prior to surface treatment.

2.2. Superhydrophilic surface treatment

The process for the superhydrophilic surface treatment of TFN has been previously described [18]. Briefly, thin films of nitinol were placed into a buffered oxide etchant (BOE: aqueous NH_4—HF etchant) to eliminate the native oxide layer followed by passivation in 30% nitric acid (HNO_3) for 40 min. Samples underwent a final oxidation process by immersion in 30% H_2O_2 for 15 h at room temperature. The surface treated TFN was stored in deionized water prior to testing. The films produced using this process have a wetting contact angle of 0° whereas the fabricated cleaned films have wetting contact angle of approximately 65°. Previous studies using transmission electron microscopy have demonstrated that the surfaced treatment produces a surface layer of TiO 100 nm thick, whereas the untreated film has a TiO_2 10 nm in thickness [21].

2.3. Creation of covered stents and in vitro flow loop circulation model

Covered stents were manufactured by producing rectangular sheets of UTFN, STFN, and ePTFE with dimensions of 1.0 cm × 0.5 cm. All coverings were weighed to an accuracy of 0.1 mg. The coverings were then deployed circumferentially in silicone tubing with an inner diameter of 3.125 mm. The coverings were deployed so that the longer 1.0 cm dimension was conformal with the tube. Next, Wingspan stents (Boston Scientific, Natick, MA) with a length of 20 mm and a diameter of 4.5 mm were deployed inside the coverings such that the center of the stent aligned with the center of the covering. A schematic diagram of the *in vitro* circulation model can be seen in Fig. 1. The silicone segments containing the deployed stents were connected in series to a length of silicone tubing placed within the head of a peristaltic roller pump (Ismatec BVP 115 V pump drive system with model 380-AD single channel pump head, Glattbrugg, Switzerland). This created a continuous loop of silicone tubing approximately 60 cm in length. Of note, the compressed section gap on the pump was set to the least occlusive setting in an effort to minimize blood trauma during circulation. The majority of the loop, including the portion containing the covered stent, was placed in a 37 °C waterbath. Phosphate buffered saline (PBS) was introduced into the loop via a 3-way stopcock and circulated at a rate of 10 mL/min for 5 min While the PBS was circulating, 15 mL of fresh whole blood was collected via venipuncture from healthy adult volunteers who reported no use of anticoagulants or other drugs within the past 2 weeks. After circulating the PBS for 5 min, the loop was disconnected at the 3-way stopcock and the syringe containing the blood was connected to the stopcock's open port. The free end of the loop was placed in a waste basin and the blood was then gently introduced into the flow loop without the addition of any anticoagulants. Though the loop's total volume was approximately 4.6 mL, all 15 mL of collected blood was injected into the loop prior to circulation to ensure complete washout of the PBS. Excess blood and PBS were collected in the waste basin from the loop's free end and disposed of using appropriate procedures. Once the loop was filled, the loop was reconnected and the blood was circulated at a rate of 6.6 mL/s. This rate was chosen because it corresponds to a wall shear rate (WSR) of 2100 s^{-1} at the surface of the stent, which correlates to shear rates observed in moderate arterial stenoses [22]. WSR is given by the equation:

$$\mathrm{WSR} = \frac{4Q}{\pi R^2}$$

where Q is equal to flow in mL/sec. and R is the radius in cm. After 3 h, the blood was drained from the loop and PBS was again circulated at 10 mL/min for 5 min to remove any non-adherent thrombus. Of note, the blood was generally free from thrombi after 3 h of circulation. Following this, the stents were removed from the silicone tubing and the coverings were unwrapped from the stents for further testing.

2.4. Scanning electron microscopy

To prepare samples for scanning electron microscopy (SEM), they were fixed in a solution of 2.5% glutaraldehyde, 1% osmic acid at 4 °C for 1 h. After 1 h, samples underwent serial dehydration in solutions of increasing ethanol concentration (50%, 60%, 70%, 80%, 90%, 95%, 100%) twice for 10 min each. Once dehydrated, the samples underwent critical-point drying overnight and were subsequently analyzed using scanning electron microscopy. Images were chosen at random and represent approximately 0.01 mm^2 of surface area.

2.5. Total blood product deposition

To calculate total blood product deposition, coverings were removed from the circulation model and excess liquid was removed via capillary action by carefully applying all edges of the covering to an absorbent surface. After all excess liquid was removed, the coverings were weighed again to an accuracy of 0.1 mg and the original weight was subtracted from this value to calculate change in weight due to blood product deposition.

2.6. Fibrin deposition

The process used for quantification of fibrin in experimentally generated thrombi has been described previously [23]. After

Please cite this article in press as: Kealey CP, et al., *In vitro* hemocompatibility of thin film nitinol in stenotic flow conditions, Biomaterials (2010), doi:10.1016/j.biomaterials.2010.08.014

removal from the flow loop, coverings were immersed in 2 mL of a plasmin solution (0.5 CU/mL, Innovative Research Inc., Novi, MI) diluted in PBS containing 1 mM Tris/HCl, pH 7.4. The coverings were then incubated at 37 °C with gentle rocking at 50 rev/min for 30 min. Following plasmin digestion, the samples were removed and the solution was collected. The solution was then centrifuged at 4300 × g for 15 min at 4 °C and the supernatant was collected. Fibrin degradation products were then quantified in the supernatant using a commercially available enzyme linked immunosorbent assay (Asserachrom D-Di, Stago, Parsippany, NJ). Total mg/cm^2 of graft material was then calculated from the solution's concentration.

2.7. Platelet deposition

Platelet deposition was quantified using fluorescent labeling of platelets with Calcein AM (Invitrogen, Carlsbad, CA). For these studies, a stock solution of Calcein AM was added to the syringe prior to drawing blood for use in the *in vitro* circulation model, such that the final concentration was 15 μM. The blood was then inoculated into the circulation model in the usual manner described above. After 3 h, the coverings were removed for analysis. Fluorescent images were obtained using a Photometrics CoolSNAP HQ2 CCD camera mounted on a Nikon Eclipse Ti Microscope. Qualitative analysis was performed by comparing representative images amongst the three materials. Quantitative analysis was performed using a custom MATLAB script. Raw color images were converted to binary data using an identical threshold level. The summation of fluorescent intensity for each data set was used as a proxy for total platelet adherence. Average fluorescent intensity for 10 randomly selected fields of view was then calculated.

2.8. Mass spectrometry

The acellular protein supernatant used for fibrin quantification, was subsequently dried in to a pellet using vacuum centrifugation. Dried sample pellets were then prepared for LC-MS/MS analysis using a previously described protocol [24]. Briefly, dried sample pellets were solubilized in 40 mM Tris–HCl pH 8.3, 6 M guanidine HCl, 5 mM DTT, centrifuged (15,000 × g, 2 min, RT), and supernatant diluted to <1 M guanidine HCl with 40 mM Tris–HCl pH 8.3. The sample was sequentially treated with DTT, iodoacetamide, and trypsin (overnight, 37 °C) according to the manufacturers protocol (Promega, Madison, WI). The pH was adjusted to pH 3 with formic acid, washed on a C18 spin column (The Nest Group, Inc.), eluted and speed vacuum dried. Dried samples were re-dissolved in Buffer A (H_2O/acetonitrile/formic acid, 98.9/1/0.1, 50 μl), separated by nanospray LC (Eskigent technologies, Inc. Dublin, CA), and analyzed by LTQ Orbitrap (Thermo Fisher) online tandem mass spectrometry. Aliquots were injected (5 μl) onto a reverse phase column (New Objective C18, 15 cm, 75 μM diameter, 5 μm particle size equilibrated in Buffer A) and eluted (300 nL/min) with an increasing concentration of Buffer B (acetonitrile/water/formic acid, 98.9/1/0.1; min 0/5, 10/10, 112/40, 130/60, 135/90, 140/90). Eluted peptides were analyzed by MS and data-dependent MS/MS acquisition (collision-induced dissociation CID), previously optimized for samples, selecting the 7 most abundant precursor ions for MS/MS with a dynamic exclusion duration of 15.0 s.

The mass spectra were searched against a human trypsin indexed database similar to that used by Whelan et al. [24], with variable modifications of carboxyamidomethylation and methionine oxidation using the Bioworks software (Thermo Fisher) based on the SEQUEST algorithm. Quantitative data analysis was performed using the Scaffold 3.0 (Proteome Software, Inc.) software program. The Bioworks search results were uploaded into the scaffold software program and a filter with a 99% minimum protein ID probability (calculated probability of correct protein identification), with a minimum number of 2 unique peptides for one protein, and with a minimum peptide ID probability of 99.9% was set. Scaffold normalizes MS/MS data between samples with similar total protein amounts allowing a comparison of protein abundance between samples. Three replicate experiments were performed for each condition. Normalization consists of averaging the spectral counts for all the samples and then multiplying the spectral counts in each sample by the average divided by the individual sample's sum.

2.9. Statistical analysis

Results of experiments are expressed as means ± standard error of mean. Data was analyzed using one-way analysis of variance (ANOVA) testing between the three sample groups (ePTFE, UTFN, STFN). Results with $p < 0.05$ were considered to be statistically significant.

3. Results

3.1. Scanning electron microscopy

Qualitative analysis of scanning electron microscopy data showed markedly increased blood product deposition on ePTFE as compared to either UTFN or STFN. The deposited product was dense, making the morphology of individual components difficult to discern. In contrast, UTFN showed a markedly decreased density of blood product deposition. The deposit was composed of both fibrin and platelets with occasional red and white blood cells visible as well. STFN also showed markedly reduced blood product deposition as compared to ePTFE but had a noticeably denser fibrin layer than that observed on UTFN. Platelet, red and white blood cell deposition was comparable to that observed on UTFN (Figs. 1 and 2).

3.2. Total blood product, fibrin, and platelet deposition

ePTFE showed the greatest amount of blood product deposition as evidenced by an average weight change of 6.3 ± 0.8 mg/cm^2 after exposure to the *in vitro* circulation model. UTFN had the second highest amount of blood product deposition at 4.5 ± 2.3 mg/cm^2. STFN showed the lowest amount of blood product deposition at 2.9 ± 0.4 mg/cm^2 ($n = 12$, $p < 0.01$) (Fig. 3A). Fibrin deposition was greatest on ePTFE with 325.9 ± 42 μg/cm^2. STFN had the second highest amount of fibrin deposition with 194.1 ± 25 μg/cm^2. Finally UTFN showed the lowest amount of fibrin deposition with 45.6 ± 7.4 μg/cm^2 ($n = 12$, $p < 0.01$) (Fig. 3B). Platelet deposition was analyzed both qualitatively (representative fluorescence microscopy images) and quantitatively (average fluorescent intensities). Quantitative analysis of platelet deposition was obtained by measuring average fluorescent intensity across ten random images from each group. ePTFE had greatly increased levels of fluorescence as compared to either of the thin films. Average intensity for ePTFE was 79,000 ± 20,000 AU/mm^2. Average intensity for UTFN was 810 ± 190 AU/mm^2, and for STFN the value was 1600 ± 440 AU/mm^2 ($n = 10$, $p < 0.01$) (Fig. 3C). Qualitative images show markedly greater amounts of platelet deposition on ePTFE than either UTFN or STFN. UTFN tended towards small groups of aggregated platelets, whereas STFN tended towards a more evenly distributed network of platelet deposition, giving rise to a "speckled" appearance (Fig. 4).

3.3. Mass spectrometry

Mass spectrometry was used to analyze the acellular portion of the plasmin-digested thrombi. The number of proteins, unique

Please cite this article in press as: Kealey CP, et al., *In vitro* hemocompatibility of thin film nitinol in stenotic flow conditions, Biomaterials (2010), doi:10.1016/j.biomaterials.2010.08.014

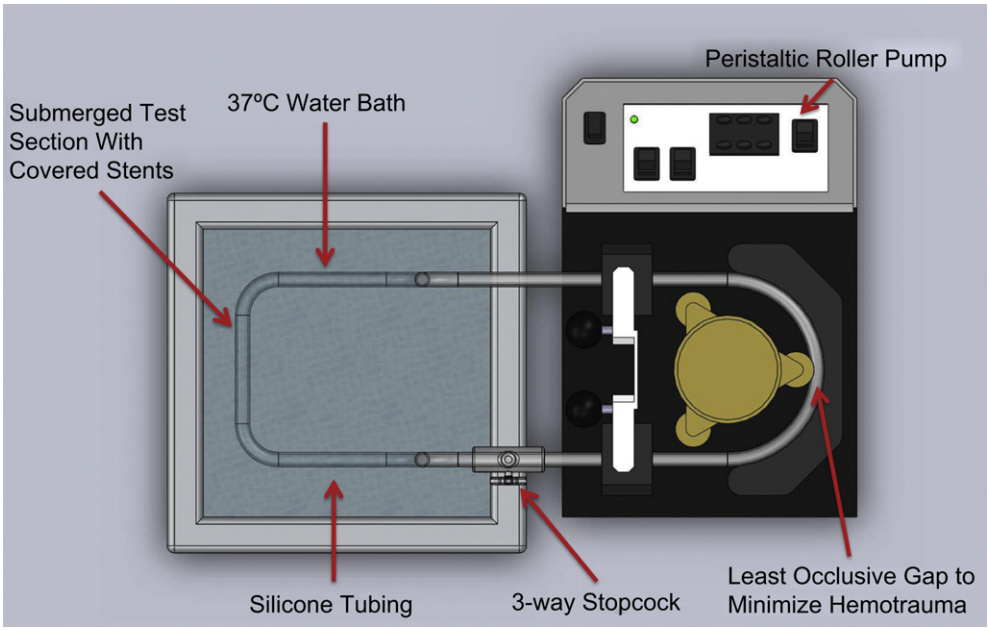

Fig. 1. Schematic representation of the *in vitro* circulation model. Blood is introduced in to a continuous loop of silicone tubing submerged in a 37 °C waterbath via a 3-way stopcock. A peristaltic roller pump propels the blood through a test section containing the covered stents. Fresh whole blood without anticoagulation was circulated through the loop for 3 h at a wall shear rate of 2200 s^{-1}.

peptides and unique spectra was compared across the 3 materials. In each case ePTFE had the greatest number, followed by STFN, the UTFN (Fig. 5A). The protein with the highest abundance in each of the samples was the fibrin α chain. Fig. 5B shows a representative spectrum for this protein, and indicates the high quality of the data. Next, our analysis turned to differences in individual protein deposition amongst the 3 materials as quantified by the number of spectral counts. Plasmin was used as the positive control because an equal amount was added to each sample. Average spectral counts per sample were the following: ePTFE 58 ± 5.8, UTFN 61 ± 14, STFN 60 ± 10 ($n = 3$, $p = 0.95$) (Fig. 6F). Other proteins examined include the α, β, and γ chains of fibrin as well as the α and β chains of hemoglobin. For fibrin, the data is reported for ePTFE, UTFN, and STFN, respectively and is as follows: α chain 119 ± 11, 38 ± 18, 90 ± 59 ($n = 3$, $p = 0.33$) (Fig. 6A). β chain 14 ± 11, 0 ± 0, 0 ± 0 ($n = 3$, $p < 0.01$) (Fig. 6B) γ chain 5.3 ± 11, 1 ± 1, 3.3 ± 3.5 ($n = 3$, $p = 0.146$) (Fig. 6C) For hemoglobin the data is as follows: α chain, 54.3 ± 3.8, 6.3 ± 6.5, 7.3 ± 2.9 ($n = 3$, $p < 0.01$) (Fig. 6D). β chain, 81 ± 3.8, 14 ± 2.6, 34 ± 7.6 ($n = 3$, $p < 0.01$) (Fig. 6E).

3.4. Flow separation zones

A consistent finding throughout this study was the preferential accumulation of thrombus at the edges of stent struts and on the stents themselves in regions where the leading edge changes its angle to the blood flow. The increased amount of thrombus at the stent edges was observed on all materials tested but was consistently greater on ePTFE than either of the thin films (Fig. 7).

4. Discussion

In this study we constructed an *in vitro* circulation model using whole blood to simulate the *in vivo* thrombotic response to thin film nitinol with ePTFE serving as control. For these studies, non-anticoagulated blood circulating at a wall shear rate similar to that found in a moderate arterial stenosis was used. An additional level of realism was added to our model by using prototype covered stents, as opposed to the bare material, because stents are known to cause local flow disturbances that influence patterns of thrombosis.

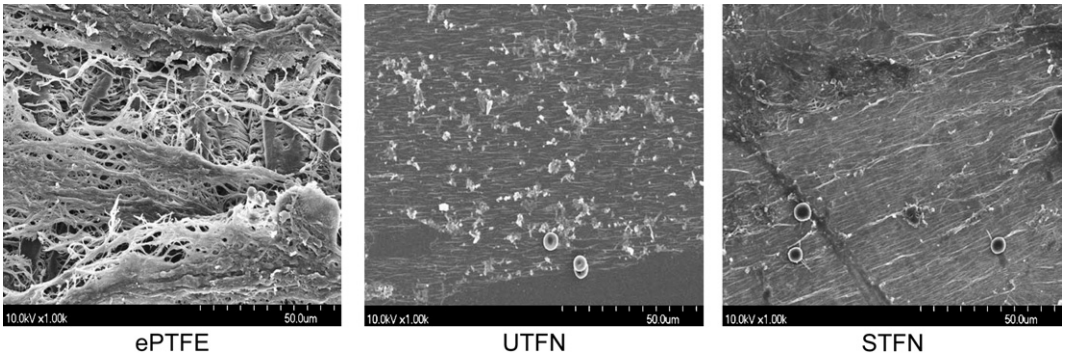

Fig. 2. Representative SEM images of the 3 materials after exposure to the *in vitro* circulation model. Images were taken randomly at 1000× magnification. ePTFE shows a dense network of blood product deposition. UTFN shows fibrin deposition and platelet aggregation. STFN shows a denser fibrin deposition that UTFN and a more evenly distributed platelet deposition.

Please cite this article in press as: Kealey CP, et al., *In vitro* hemocompatibility of thin film nitinol in stenotic flow conditions, Biomaterials (2010), doi:10.1016/j.biomaterials.2010.08.014

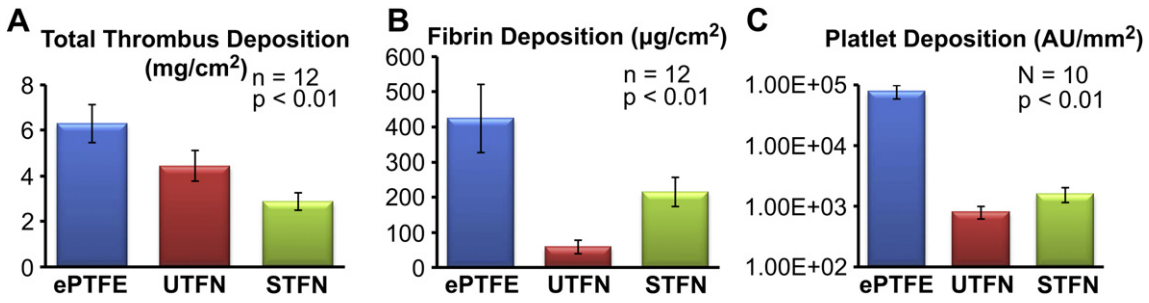

Fig. 3. A) Total blood product deposition as measured by change in weight (mg/cm^2) after exposure to the *in vitro* circulation model for 3 h at a wall shear rate of 2200 s^{-1}. B) Fibrin deposition ($\mu g/cm^2$) measured by ELISA. C) Platelet deposition (AU/mm^2) measured using fluorescently labeled platelets, log scale. Note that ePTFE has the greatest amount of total blood product, fibrin, and platelet deposition as compared to either untreated or superhydrophilic TFN.

We report that TFN (both superhydrophilic surface treated and non-surface treated) showed less blood product deposition than ePTFE by all modalities used to examine the thrombotic response.

It is widely agreed that the first event in blood-biomaterial contact is a rapid adsorption of protein on to the biomaterial's surface. Adsorbed proteins then interact with other blood components in a process that determine both the quality and quantity of thrombus formation [25]. Factors known to influence this process include surface roughness, surface charge, surface energy and contact wetting angle. With regard to surface roughness, it has been demonstrated that as this parameter increases, so too does protein adsorption, cell adhesion, and the thrombotic response [26–29]. This is likely due to both the increased number of binding sites as well as the more turbulent local flow conditions caused by rougher materials. We have previously reported that the average peak to valley surface roughness of our TFN is 5 nm, whereas that measured for ePTFE is approximately 20 μm [11,18]. We propose that this reduction in surface roughness of greater than 3 orders of magnitude significantly reduces protein adsorption and cell adhesion, thus improving TFN's hemocompatibility.

The quality of the titanium oxide layer formed on the surface of TFN is another important factor that likely increases its hemocompatibility. While the surface of untreated TFN is composed of a layer of TiO_2 10 nm thick, the superhydrophilic treatment process yields a TiO layer 100 nm in thickness [21]. Previous studies regarding the hemocompatibility of titanium oxide films have concluded that the low interface tension between TiO films and blood provides an insulating cushion that prevents protein adhesion and clotting cascade activation [30].

In order to better understand the characteristics of the thrombi forming on the surface of TFN, we developed assays for the quantification of fibrin and platelets. The fibrin assay made use of an ELISA that allowed us to quantify fibrin deposition per unit area. This assay demonstrated that fibrin deposition was greatest on ePTFE, followed by STFN, but that UTFN had the least. The increased deposition of fibrin on STFN as compared to UTFN is consistent with a large body of work showing that hydrophilic materials activate the intrinsic arm of the clotting cascade [31–33]. The *in vivo* effects of increased fibrin deposition on STFN are not clear as fibrin acts as a scaffold for both thrombus formation and endothelial cell adhesion and proliferation. It is conceivable that increased fibrin deposition on STFN may facilitate one or both of these processes. Studies examining rates of acute stent thrombosis, speed of endothelial coverage, and degree of neointimal hyperplasia as compared to UTFN are presently being investigated using *in vivo* models.

Platelet adhesion was examined using fluorescently labeled platelets. Both qualitative and quantitative data show increased platelet adhesion on ePTFE. Overall platelet fluorescence was more than 2 orders of magnitude larger on ePTFE than on either thin film. Additionally, a consistent "halo" of background fluorescence was observed on all ePTFE samples that we believe represents platelets caught within the woven polymer fibers. This effect was absent on TFN and highlights the advantage of our film's smooth, metallic surface. Because platelets are the primary mediator of acute stent thrombosis, we hope that the marked reduction in platelet adhesion seen *in vitro* will extend to *in vivo* results [34,35].

A surprising finding from this study was the increased platelet deposition on STFN as compared to UTFN. Though the difference between the two films was minor compared to the difference with ePTFE, there were both a qualitatively different pattern of platelet distribution (small aggregates on UTFN, uniformed "speckling" on STFN) as well as a quantitative finding of increased fluorescence

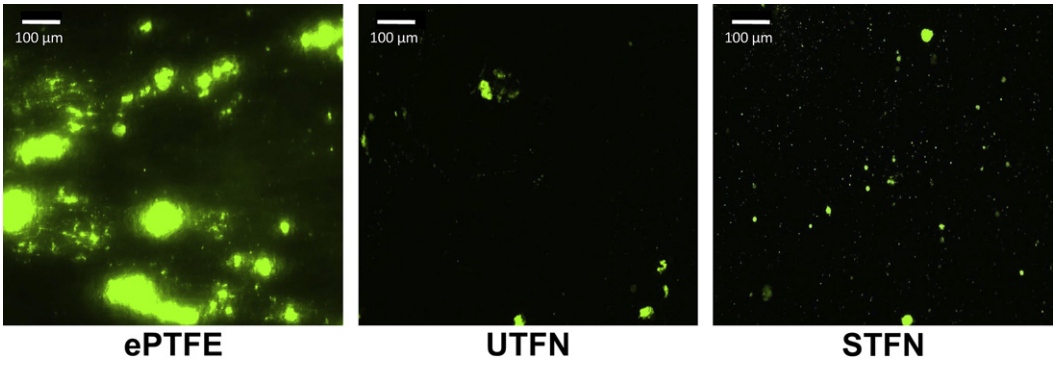

Fig. 4. Fluorescent images of platelet deposition on the 3 materials after exposure to the *in vitro* circulation model. ePTFE showed large clusters of aggregated platelets and a halo effect of background fluorescence likely due to trapped platelets within the woven polymer fibers. UTFN tended towards smaller clusters of aggregated platelets. STFN showed a more evenly distributed platelet network, giving a "speckled" appearance.

Please cite this article in press as: Kealey CP, et al., *In vitro* hemocompatibility of thin film nitinol in stenotic flow conditions, Biomaterials (2010), doi:10.1016/j.biomaterials.2010.08.014

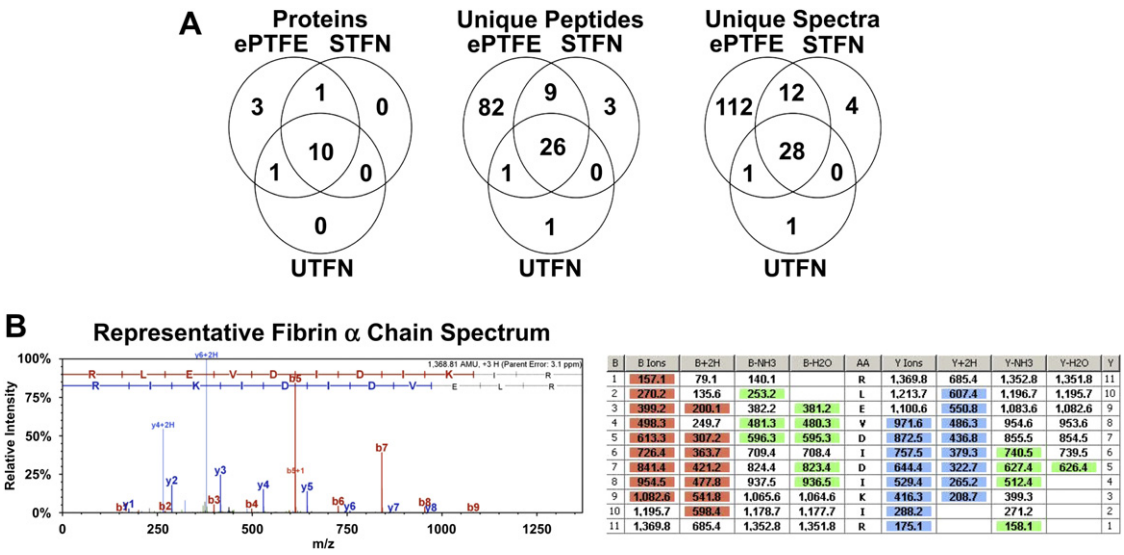

B	B Ions	B+2H	B-NH3	B-H2O	AA	Y Ions	Y+2H	Y-NH3	Y-H2O	Y
1	157.1	79.1	140.1		R	1,369.8	685.4	1,352.8	1,351.8	11
2	270.2	135.6	253.2		L	1,213.7	607.4	1,196.7	1,195.7	10
3	399.2	200.1	382.2	381.2	E	1,100.6	550.8	1,083.6	1,082.6	9
4	498.3	249.7	481.3	480.3	V	971.6	486.3	954.6	953.6	8
5	613.3	307.2	596.3	595.3	D	872.5	436.8	855.5	854.5	7
6	726.4	363.7	709.4	708.4	I	757.5	379.3	740.5	739.5	6
7	841.4	421.2	824.4	823.4	D	644.4	322.7	627.4	626.4	5
8	954.5	477.8	937.5	936.5	I	529.4	265.2	512.4		4
9	1,082.6	541.8	1,065.6	1,064.6	K	416.3	208.7	399.3		3
10	1,195.7	598.4	1,178.7	1,177.7	I	288.2		271.2		2
11	1,369.8	685.4	1,352.8	1,351.8	R	175.1		158.1		1

Fig. 5. Mass spectrometry data. A) Venn diagrams showing the number of proteins, unique peptides, and unique spectra of each of the three materials. ePTFE had the largest amount for each parameter. B) A representative spectrum of the fibrin α chain.

intensity on STFN. This is in direct contrast to earlier studies using PRP under static conditions. These studies showed markedly reduced platelet adhesion on STFN as compared to UTFN [19]. These findings were thought to be explained by the superhydrophilic surface treatment of STFN because platelet adhesion is known to decrease with increasing hydrophilicity [36]. It is likely that the results presented here are different because of the increased fibrin deposition on STFN due to the hydrophilic activation of the intrinsic clotting cascade. Fibrin depositing on the superhydrophilic surface is serving as a scaffold for platelet adhesion, thus overcoming the tendency of hydrophilic surfaces to repel platelets. This PRP used in the static experiments is known to yield a solution low in fibrin content, and one can see from the SEM images in that study that no fibrin is apparent on any of the analyzed surfaces [19,37]. This explanation also accounts for the more homogenous, or "speckled" distribution of platelets on STFN that would be expected if the platelets are attaching to an evenly distributed fibrin network.

Mass spectrometry was used to analyze the acellular component of the plasmin-digested thrombi. These results confirm findings from the other assays, and show that ePTFE bound a greater number of unique proteins, peptides, and spectral counts than either of the thin films. More specifically, ePTFE exhibited greater amounts of the α, β, and γ chains of fibrin confirming the results obtained from our ELISA assay for fibrin concentration. Mass spectrometry also demonstrated increased amounts of the α, β chains of hemoglobin on ePTFE. This strongly suggests that ePTFE attracts increased red blood cell deposition in addition to the other quantified thrombotic components.

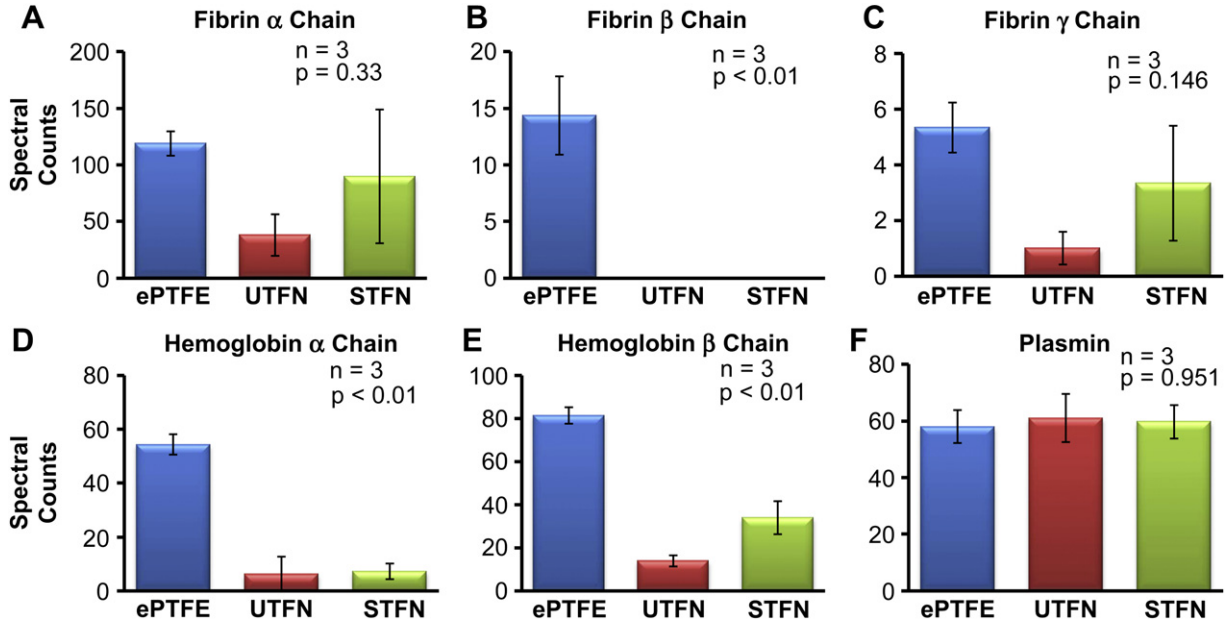

Fig. 6. Mass spectrometry data showing average spectral counts for six different proteins. A) fibrin α chain B) fibrin β chain C) fibrin γ chain D) Hemoglobin α chain E) Hemoglobin β chain F) Plasmin (positive control). This data confirms the trend in fibrin deposition measured by ELISA. Additionally, increased hemoglobin deposition on ePTFE suggests a larger amount of RBCs depositing on this material than either of the thin films.

Please cite this article in press as: Kealey CP, et al., *In vitro* hemocompatibility of thin film nitinol in stenotic flow conditions, Biomaterials (2010), doi:10.1016/j.biomaterials.2010.08.014

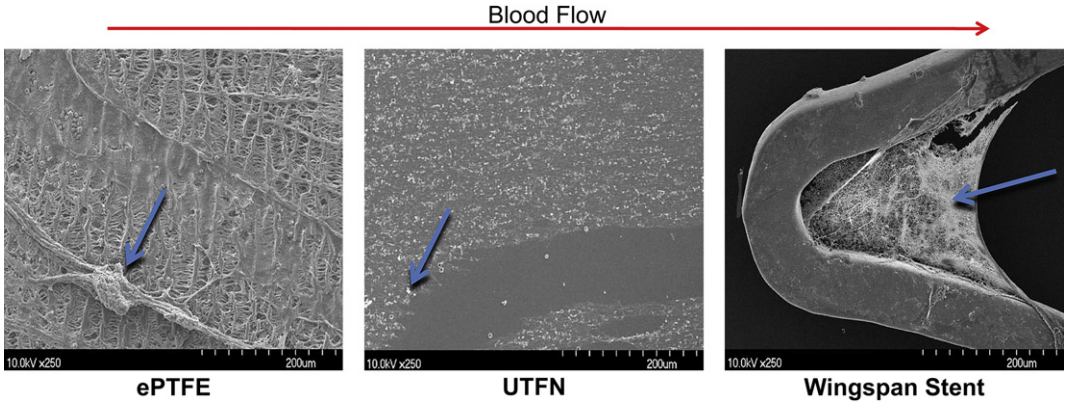

Fig. 7. Flow separation zones are areas of significant thrombus accumulation. Blue arrows represent areas of preferential thrombus formation in the peri-strut region. ePTFE shows dense thrombus accumulation all along the stent edge. In the UTFN sample, the stent edge is clearly seen but the dense accumulations observed on ePTFE are absent. The Wingspan stent strut shows preferential thrombus accumulation around strut edges and in areas where the stent changes direction relative to blood flow. These regions create flow separation and blood product deposition.

An interesting result of these experiments was the visualization of thrombus formed preferentially around the stent struts and in areas where the struts change direction relative to the blood flow. Over the past decade, there has been a modest but growing body of literature regarding the flow disturbances induced by stent placement [38–40]. Most of these studies have used computational fluid dynamics simulations to visualize these disturbances. A unique advantage of this study was that the stent coverings functioned like a photographic negative of the stent, allowing us to visualize the patterns of thrombus deposition around the struts. Notably, while all materials were exposed to the same local flow environments, the thin film performed markedly better than the ePTFE, lacking the dense thrombotic deposits in the peri-strut regions. We believe that these results are significant and provide strong experimental evidence that stent design to encourage laminar flow and normalization of wall shear stress should be an area of active investigation.

The *in vitro* circulation model used for these experiments provides a quick and efficient test system to simulate *in vivo* interactions between endovascular devices and whole human blood under flow conditions. While we believe the information provided by this model is both useful and significant, the limitations of this system must also be considered. First and foremost, there is no endothelium. It is well known that endothelial cells mediate interactions between blood and the vessel wall, and that damage to the endothelium leads to activation of both platelets and the clotting cascade [41]. While other authors have used similar circulation models, they examined the effects of different stents on activation of blood components such as platelets and leukocytes [42,43]. They concluded that maximum activation of the blood occurred after 30 min of circulation and plateaued thereafter. Additional problems with this model include the relatively large surface area of silicone tubing in contact with the blood, as well as the use of a peristaltic pump head for tube compression which can lead to hemolysis and thrombosis. Therefore, it seems reasonable to conclude that the circulating blood used in this study was highly activated. This likely led to a large amount of non-specific clotting that would not be observed in an *in vivo* system making definitive judgments about relative hemocompatibilities of the different materials difficult. Along these lines, we anticipate questions about both the use of non-anticoagulated blood and the relatively long circulation time of 3 h. Initial testing with this system used ACD anti-coagulated blood and a circulation time of 30 min. These conditions, however, failed to elicit significant thrombus deposition on all of the coverings being tested, and a system of trial and error determined the optimum conditions chosen to elicit significant differences between the materials. In this study, we chose to examine thrombus accumulation as opposed to overall blood activation based on the assumption that the system itself will maximally activate the blood after 30 min. By including all three types of covered stents in each loop, we exposed all three materials to the same conditions, thus providing an internal control. Therefore, while one cannot directly correlate these results to *in vivo* performance, they suggest that both thin films attract significantly less thrombus deposition than ePTFE under highly thrombogenic conditions.

5. Conclusion

The purpose of this study was to compare the hemocompatibility profiles of ePTFE, UTFN and STFN in an *in vitro* circulation model using fresh whole human blood under conditions simulating a moderate arterial stenosis. A series of assays to qualitatively and quantitatively analyze the experimentally formed thrombi were developed. This data suggests that both forms of TFN tested attract significantly less thrombus than ePTFE under the highly thrombogenic experimental conditions. Our previous work has demonstrated the feasibility of constructing TFN covered stents and we have successfully placed them *in vivo*. Additional advantages of TFN include the ability to micropattern its surface, and the ability to make extremely low-profile transcatheter devices. As stent graft technology advances, there will be a need for less thrombogenic, less bulky materials that facilitate rapid healing and incorporation in to the vessel wall. The current study, combined with our previous work, suggests that TFN is an excellent candidate material.

Acknowledgements

This work was supported by NIH challenge grant number 1RC1HL099445-01

Appendix

Figures with essential color discrimination. Figs. 1,3–7 in this article are difficult to interpret in black and white. The full color images can be found in the online version, at doi:10.1016/j.biomaterials.2010.08.014.

References

[1] Ansel G, Lumsden A. Evolving modalities for femoropopliteal interventions. J Endovasc Ther 2009;16(Suppl. II):82–97.

[2] Chambers D, Epstein D, Walker S, Fayter D, Paton F, Wright K, et al. Endovascular stents for abdominal aortic aneurysms: a systematic review and economic model. Health Technol Assess 2009;13(48).

[3] Wilt TJ, Lederle FA, MacDonald R, Jonk YC, Rector TS, Kane RL. Comparison of endovascular and open surgical repairs for abdominal aortic aneurysm. Evidence Report/Technology Assessment No. 144. (Prepared by the University of Minnesota Evidenced Based Practice Center under Contract No. 290-02-0009.) AHRQ Publication No. 06-E017. Rockville, MD: Agency for Healthcare Research and Quality; 2006.

[4] Cheng D, Martin J, Shennib H, Dunning J, Muneretto C, Schueler S, et al. Endovascular aortic repair versus open surgical repair for descending thoracic aortic disease a systematic review and meta-analysis of comparative studies. J Am Coll Cardiol 2010;55(10):986–1001.

[5] Bauermeister G. Endovascular stent-grafting in the treatment of superficial femoral artery occlusive disease. J Endovasc Ther 2001;8(3):315–20.

[6] Fischer M, Schwabe C, Schulte KL. Value of the hemobahn/viabahn endoprosthesis in the treatment of long chronic lesions of the superficial femoral artery: 6 years of experience. J Endovasc Ther 2006;13(3):281–90.

[7] Kedora J, Hohmann S, Garrett W, Munschaur C, Theune B, Gable D. Randomized comparison of percutaneous Viabahn stent grafts vs prosthetic femoral-popliteal bypass in the treatment of superficial femoral arterial occlusive disease. J Vasc Surg 2007;45(1):10–6.

[8] Saxon RR, Dake MD, Volgelzang RL, Katzen BT, Becker GJ. Randomized, multicenter study comparing expanded polytetrafluoroethylene-covered endoprosthesis placement with percutaneous transluminal angioplasty in the treatment of superficial femoral artery occlusive disease. J Vasc Inter Radiol 2008;19(6):823–32.

[9] Saxon RR, Coffman JM, Gooding JM, Ponec DJ. Long-term patency and clinical outcome of the Viabahn stent-graft for femoropopliteal artery obstructions. J Vasc Interv Radiol 2007;18(11):1341–9.

[10] Alimi YS, Hakam Z, Hartung O, Boufi M, Barthelemy P, Aissi K, et al. Efficacy of Viabahn in the treatment of severe superficial femoral artery lesions: which factors influence long-term patency? Eur J Vasc Endovasc Surg 2008;35:346–52.

[11] Hallab NJ, Bundy KJ, O'Connor K, Moses RL, Jacobs JJ. Evaluation of metallic and polymeric biomaterial surface energy and surface roughness characteristics for directed cell adhesion. Tissue Eng 2001;7(1):55–71.

[12] Rigberg D, Tulloch A, Chun Y, Mohanchandra KP, Carman G, Lawrence P. Thin-film nitinol (NiTi): a feasibility study for a novel aortic stent graft material. J Vasc Surg 2009;50(2):375–80.

[13] Marin ML, Veith FJ, Cynamon J, Sanchez LA, Schwartz ML, Lyon RT, et al. Human transluminally placed endovascular stented grafts: preliminary histopathologic analysis of healing grafts in aortoiliac and femoral artery occlusive disease. J Vasc Surg 1995;21(4):595–603.

[14] Marin ML, Veith FJ, Cynamon J, Parsons RE, Lyon RT, Suggs WD, et al. Effect of polytetrafluoroethylene covering of Palmaz stents on the development of intimal hyperplasia in human iliac arteries. J Vasc Interv Radiol 1996;7(5):651–6.

[15] Zilla P, Deutsch M, Meinart J, Puschmann R, Eberl T, Minar E, et al. Clinical *in vitro* endothelialization of femoropopliteal bypass grafts: an actuarial follow-up over three years. J Vasc Surg 1995;19(3):549–54.

[16] Shabalovskaya SA. On the nature of the biocompatibility and on medical applications of NiTi shape memory and superelastic alloys. Biomed Mater Eng 1996;6(4):267–89.

[17] Stepan LL, Levi DS, Gans E. Biocorrosion investigation of two shape memory nickel based alloys: Ni-Mn-Ga and thin film NiTi. J Biomed Mater Res A 2007;82(3):768–76.

[18] Chun Y, Levi DS, Mohanchandra KP, Carman GP. Superhydrophilic surface treatment for thin film NiTi vascular applications. Mater Sci Eng C 2009;29(8):2436–41.

[19] Tulloch AW, Chun Y, Levi DS, Mohanchandra KP, Carman GP, et al. Superhydrophilic thin film nitinol demonstrates reduced platelet adhesion compared with commercially available endograft materials. J Surg Res 2010:1–6.

[20] Ho KK, Carman GP. Sputter deposition of NiTi thin film shape memory alloy using a heated target. J Thin Solid Films 2000;370:18–29.

[21] Mohanchandra KP, Chun YJ, Kealey CP, Tulloch AW, Lin S, Rigberg DA, et al. TEM studies on surface treated Ni-Ti thin films. In press.

[22] Malek AM, Schirmer CM. Wall shear stress gradient analysis within an idealized stenosis using non-Newtonian flow. Neurosurgery 2007;61(4):853–63.

[23] Orvim U, Barstad RM, Stormorken H, Brosstad F, Sakariassen KS. Immunologic quantification of fibrin deposition in thrombi formed in flowing native human blood. Br J Haematol 1996;95:389–98.

[24] Whelan SA, He ML, Yan W, Faull KF, Whitelegge JP, Saxton RE, et al. Mass spectrometry (LC-MS/MS) site-mapping of N-glycosylated membrane proteins for breast cancer biomarkers. J Proteome Res 2009;8(8):4151–60.

[25] Courtney JM, Lamba NMK, Sundaram S, Forbes CD. Biomaterials for blood-contacting applications. Biomaterials 1994;15(10):737–44.

[26] Thierry B, Tabrizian M. Biocompatibility and biostability of metallic endovascular implants: state of the art and perspectives. J Endovasc Ther 2003;10(4):807–24.

[27] Park JY, Gemmell CH, Davies JE. Platelet interactions with titanium: modulation of platelet activity by surface topography. Biomaterials 2001;22:2671–82.

[28] De Scheerder I, Verbeken E, Van Humbeeck J. Metallic surface modification. Semin Interv Cardiol 1998;3(3–4):139–44.

[29] Xu LC, Siedlecki CA. Effects of surface wettability and contact time on protein adhesion on biomaterial surfaces. Biomaterials 2007;28:3273–83.

[30] Huang N, Yang P, Leng YX. Hemocompatibility of titanium oxide films. Biomaterials 2003;24(13):2177–87.

[31] Zhuo R, Miller R, Bussard KM, Siedlecki CA, Vogler EA. Procoagulant stimulus processing by the intrinsic pathway of blood plasma coagulation. Biomaterials 2005;26:2965–73.

[32] Vogler EA, Graper JC, Harper GR, Lander LM, Brittain WJ. Contact activation of the plasma coagulation cascade. 1. Procoagulant surface energy and chemistry. J Biomed Mater Res 1995;29:1005–16.

[33] Vogler EA, Graper JC, Harper GR, Lander LM, Brittain WJ. Contact activation of the plasma coagulation cascade. 2. Protein adsorption on procoagulant surfaces. J Biomed Mater Res 1995;29:1017–28.

[34] Montalescot G, Barragan P, Wittenberg O, Ecollan P, Elhadad S, Villain P, et al. Platelet glycoprotein IIb/IIIa inhibition with coronary stenting for acute myocardial infarction. NEJM 2001;344:1895–903.

[35] Myung HJ, Owen WG, Staab ME, Srivatsa SS, Sangiorgi G, Stewart M, et al. Porcine model of stent thrombosis: platelets are the primary mediator of acute stent closure. Cathet Cardiovasc Diagn 1998;38(1):38–43.

[36] Palmaz J. New advances in endovascular technology. Tex Heart Inst J 1997;24:156–9.

[37] Dohan Ehrenfest DM, Rasmusson L, Albrektsson T. Classification of platelet concentrates: from pure platelet-rich plasma (P-PRP) to leucocyte- and platelet-rich fibrin (L-PRF). Trends Biotechnol 2009;27(3):158–67.

[38] Jimenez JM, Davies PF. Hemodynamically driven stent strut design. Ann Biomed Eng 2009;37(8):1483–94.

[39] He Y, Duraiswamy N, Frank AO, Moore JE. Blood flow in stented arteries: a parametric comparison of strut design patterns in three dimensions. J Biomech Eng 2005;127:637–47.

[40] Duraiswamy N, Schoephoerster RT, Moore JE. Comparison of near-wall hemodynamic parameters in stented artery models. J Biomech Eng 2009;131:061006–61011.

[41] Watson SP. Platelet activation by extracellular matrix proteins in haemostasis and thrombosis. Curr Pharm Des 2009;15:1358–72.

[42] Tepe G, Wendel HP, Korchidi S, Schmehl J, Wiskirchen J, Pusich B, et al. Thrombogenicity of various endovascular stent types: an *in vitro* study. J Vasc Interv Radiol 2002;13:1029–35.

[43] Nguyen KT, Su SH, Sheng A, Wawro D, Schwade ND, Brouse CF, et al. *In vitro* hemocompatibility studies of drug-loaded poly-(L-lactic acid) fibers. Biomaterials 2003;24:5191–201.

Please cite this article in press as: Kealey CP, et al., *In vitro* hemocompatibility of thin film nitinol in stenotic flow conditions, Biomaterials (2010), doi:10.1016/j.biomaterials.2010.08.014